

Gravitational Radiation from Axisymmetric Rotational Core Collapse

Kei Kotake,^{1,*} Shoichi Yamada,² and Katsuhiko Sato^{1,3}

*¹Department of Physics, School of Science,
the University of Tokyo, 7-3-1 Hongo,
Bunkyo-ku, Tokyo 113-0033, Japan*

*²Science & Engineering, Waseda University,
3-4-1 Okubo, Shinjuku, Tokyo, 169-8555, Japan*

*³Research Center for the Early Universe,
School of Science, the University of Tokyo,
7-3-1 Hongo, Bunkyo-ku, Tokyo 113-0033, Japan*

(Dated: November 2, 2018)

Abstract

We have done a series of two-dimensional hydrodynamic simulations of the rotational collapse of a supernova core in axisymmetry. We have employed a realistic equation of state (EOS) and taken into account electron captures and neutrino transport by the so-called leakage scheme. It is an important progress to apply the realistic EOS coupled with the microphysics to 2-D simulations for computing gravitational radiation in rotational core collapse. We have used the quadrupole formula to calculate the amplitudes and the waveforms of gravitational wave assuming the Newtonian gravity. From these computations, we have extended the conventional category of the gravitational waveforms. Our results have shown that the peak amplitudes of gravitational wave are mostly within the sensitivity range of the laser interferometers such as TAMA and first LIGO for a source at a distance of 10 kpc. Furthermore we have found that the amplitudes of the second peaks are within the detection limit of first LIGO for the source and first pointed out the importance of the detections, since they will give us the information as to the angular momentum distribution of evolved massive stars.

PACS numbers:

*E-mail: kkotake@utap.phys.s.u-tokyo.ac.jp

I. INTRODUCTION

Asymmetric core collapse and supernova have been supposed to be one of the most plausible source of gravitational radiation for the long-baseline laser interferometers (GEO600, LIGO, TAMA, VIRGO) [1]. The detection of the gravitational signal is important not only for the direct confirmation of general relativity but also for the understanding of supernovae themselves because the gravitational wave is only a window that enables us to see directly the innermost part of an evolved star, where the angular momentum distribution and the equation of state are unknown.

Observationally, the asymmetric aspects of the dynamics of supernovae are evident because they are confirmed by many observations of SN 1987A [2, 3, 4] and by the kick velocity of pulsars [5]. On the other hand, there is no consensus of the origin of asymmetry theoretically. However, provided the facts that the progenitors of collapse-driven supernovae are a rapid rotator on the main sequence [6] and that the recent theoretical studies suggest a fast rotating core prior to the collapse [7], rotation should play an important role as the origin of the asymmetric motions in the core collapse. It is noted that anisotropic neutrino radiations induced by rotation [8] could induce a jet-like explosion [9] as suggested by the observations of SN 1987A.

So far there have been works devoted to study the gravitational radiation in the rotational core collapse [10, 11, 12, 13, 14, 15, 16] (see [17] for a review). To say rigorously, reliable core collapse simulations should require the implementation of a realistic equation of state (EOS), an adequate treatment of microphysics (electron captures and other weak interactions) and neutrino transport, and a relativistic treatment of gravitation. However it is difficult to incorporate all of them at the same time. Therefore previous investigations have neglected or approximated the above requirements partially. So far most of the computations have oversimplified the microphysics. In addition, it has been reported that general relativity does not alter the significant features of gravitational radiation compared with those obtained in Newtonian approximation such as the range of gravitational wave amplitudes and frequencies [14]. This situation motivates us to employ a realistic EOS and treat microphysics adequately in the Newtonian gravity. In this paper, we will study the wave forms of gravitational radiation elaborately by performing the improved rotational core collapse simulations and will discuss what information can be extracted from the analysis.

We describe the numerical models in the next section. In the third section, we show the main numerical results. Conclusion is given in the last section.

II. MODELS AND NUMERICAL METHODS

A. Initial models

We know little of angular momentum distributions in a core of evolved massive stars. Although it is supposed that some instabilities grow and transport angular momentum during the quasi-static evolutions, which mode prevails in what time scale is not understood very well at present. Therefore, we assume in this study the following two possible rotation laws.

1. shellular rotation:

$$\Omega(r) = \Omega_0 \times \frac{R_0^2}{r^2 + R_0^2}, \quad (1)$$

where $\Omega(r)$ is an angular velocity, r is a radius, and Ω_0, R_0 are model constants.

2. cylindrical rotation:

$$\Omega(X, Z) = \Omega_0 \times \frac{X_0^2}{X^2 + X_0^2} \cdot \frac{Z_0^4}{Z^4 + Z_0^4}, \quad (2)$$

where X and Z denote distances from the rotational axis and the equatorial plane and X_0, Z_0 are model constants. The other parameters have the same meanings as above.

Although recent theoretical studies [7] give estimates for the angular velocity prior to the collapse, they are one-dimensional models with uncertainties and not the final answer. Hence we prefer a parametric approach in this paper. We have computed twelve models changing the combination of the total angular momentum, the rotation law, and the degree of differential rotation. The model parameters are presented in Table I. The models are named after this combination, with the first letter, “S (Slow)”, “M (Moderate)”, “R (Rapid)”, representing the initial $T/|W|_{\text{init}}$, the second letter, “S (Shellular), C (Cylindrical)”, denoting the rotation law, and the third letter, “L (Long), S (Short)”, indicating the values of R_0 and X_0 , which represent the degree of differential rotation. The initial ratio of rotational energy to gravitational energy is designated as $T/|W|_{\text{init}}$. We have chosen 0.25, 0.5, 1.5% for $T/|W|_{\text{init}}$. The rotational progenitor model [18] corresponds to Model MSL (Moderate, Shellular rotation, $R_0 = 1000$ km) in our simulations and we take this case

TABLE I: The Model Parameters.

Model	$T/ W _{\text{init}}(\%)$	Rotation Law	$R_0, X_0, Z_0 \times 10^8$ (cm)	Ω_0 (s^{-1})
SSL	0.25	Shellular	$R_0 = 1$	2.8
SSS	0.25	Shellular	$R_0 = 0.1$	45.1
SCL	0.25	Cylinder	$X_0 = 1, Z_0 = 1$	2.7
SCS	0.25	Cylinder	$X_0 = 0.1, Z_0 = 1$	31.3
MSL	0.50	Shellular	$R_0 = 1$	4.0
MSS	0.50	Shellular	$R_0 = 0.1$	63.4
MCL	0.50	Cylinder	$X_0 = 1, Z_0 = 1$	3.8
MCS	0.50	Cylinder	$X_0 = 0.1, Z_0 = 1$	44.4
RSL	1.50	Shellular	$R_0 = 1$	6.8
RSS	1.50	Shellular	$R_0 = 0.1$	112
RCL	1.50	Cylinder	$X_0 = 1, Z_0 = 1$	6.6
RCS	1.50	Cylinder	$X_0 = 0.1, Z_0 = 1$	76.8

as the standard model. We have made precollapse models by taking a density and internal energy distribution from the spherically symmetric $15 M_\odot$ model by Woosley and Weaver (1995) and by adding the angular momentum according to the rotation laws stated above.

B. Hydrodynamics

The numerical method for hydrodynamic computations employed in this paper is based on the ZEUS-2D code [19]. The code is an Eulerian one based on the finite-difference method and employs an artificial viscosity of von Neumann and Richtmyer to capture shocks. The self-gravity is managed by solving the Poisson equation with the Incomplete Cholesky decomposition Conjugate Gradient (ICCG) method. Spherical coordinates are used and one quadrant of the meridian section is covered with $300 (r) \times 50 (\theta)$ mesh points. The code is checked by standard tests such as the Sod shock-tube problem. We have made several major changes to the base code to include the microphysics. First we have added an equation for electron fraction to treat electron captures, which is solved separately. We

have approximated electron captures and neutrino transport by the so-called leakage scheme [20, 21, 22, 23]. Second, we have incorporated the tabulated equation of state (EOS) based on the relativistic mean field theory [24] instead of the ideal gas EOS assumed in the original code. It is noted that the implementation of the recent realistic EOS to 2-D simulations is an important progress beyond the previous calculations. For a more detailed description of the methods, see Kotake et al. [8].

C. Gravitational wave signal

We follow the methods by [10, 11] in order to compute the gravitational wave form. We will summarize it in the following for convenience. The amplitude of the gravitational wave $h_{\mu\nu} \equiv g_{\mu\nu} - \eta_{\mu\nu}$ can be calculated by the quadrupole formula as follows:

$$h_{ij}^{\text{TT}}(R) = \frac{2G}{c^4} \frac{1}{R} \frac{d^2}{dt^2} I_{ij}^{\text{TT}} \left(t - \frac{R}{c} \right), \quad (3)$$

where i, j run from 1 to 3, t is the time, R is the distance from the source to the observer, the superscript “TT” means to take the transverse traceless part, and I_{ij} is the reduced quadrupole defined as

$$I_{ij} = \int \rho(x) \left(x_i x_j - \frac{1}{3} x^2 \delta_{ij} \right) d^3x. \quad (4)$$

The second time derivative of the reduced quadrupole formula, which is difficult to be treated numerically, can be replaced by the spatial derivative by the equations of motion. In the case of axisymmetric collapse, the transverse traceless gravitational field is shown to have one independent component, $h_{\theta\theta}^{\text{TT}}$, and it is dependent solely on A_{20}^{E2} . Then one derives for the component of h^{TT} the following formula,

$$h_{\theta\theta}^{\text{TT}} = \frac{1}{8} \left(\frac{15}{\pi} \right)^{1/2} \sin^2 \theta \frac{A_{20}^{\text{E2}}}{R}, \quad (5)$$

where θ is the polar angle and A_{20}^{E2} is defined as

$$A_{20}^{\text{E2}} = \frac{G}{c^4} \frac{32\pi^{3/2}}{\sqrt{15\pi}} \int_0^1 \int_0^\infty r^2 dr d\mu \rho \left[v_r^2 (3\mu^2 - 1) + v_\theta^2 (2 - 3\mu^2) - v_\phi^2 - 6v_r v_\theta \mu \sqrt{1 - \mu^2} \right. \\ \left. - r \partial_r \Phi (3\mu^2 - 1) + 3\partial_\theta \Phi \mu \sqrt{1 - \mu^2} \right], \quad (6)$$

where $\partial_r = \partial/\partial r$, $\partial_\theta = \partial/\partial\theta$, $\mu = \cos\theta$ and Φ is the gravitational potential. Since the gravitational wave is radiated most in the equatorial plane, the observer is assumed to be located in the plane in the following discussions. In addition, the source is assumed to be located at a distance of $R = 10$ kpc.

TABLE II: Summary of important quantities for all models. t_b is the time of bounce, ρ_{maxb} is the maximum density at bounce, $M_{\text{i,c b}}$ is the mass of inner core at bounce, $T/|W|_{\text{final}}$ is the final ratio of rotational energy to gravitational energy of the core, Δt is the duration time (FWHM) of the first burst, and $|h^{\text{TT}}|_{\text{max}}$ is the maximum amplitude of the first burst. Note that we speak of the inner core, where the matter falls subsonically, which corresponds to the unshocked region after core bounce.

Model	t_b	ρ_{maxb}	$M_{\text{i,c b}}$	$T/ W _{\text{final}}$	Δt	$ h^{\text{TT}} _{\text{max}}$
	(ms)	($10^{14} \text{ g cm}^{-3}$)	(M_{\odot})	(%)	(ms)	(10^{-20})
SSL	227.4	2.95	0.74	4.87	0.58	1.03
SSS	227.3	2.80	0.75	5.66	0.54	1.49
SCL	241.2	2.87	0.75	5.09	0.46	0.93
SCS	230.7	2.84	0.73	6.46	0.56	2.00
MSL	242.7	2.65	0.75	8.44	0.72	1.58
MSS	242.2	2.15	0.87	9.05	0.57	2.03
MCL	241.9	2.85	0.76	8.38	0.70	1.53
MCS	245.4	1.45	0.91	9.94	0.51	2.87
RSL	338.7	1.21	0.94	14.6	2.89	0.48
RSS	328.6	0.53	0.96	13.3	2.80	0.78
RCL	338.4	1.36	0.95	14.5	4.47	0.42
RCS	326.7	0.18	1.11	12.3	1.91	1.41

III. NUMERICAL RESULTS

1. The Properties of the Waveform

We first show the general properties of the waveform with collapse dynamics. We choose model MSL (standard) as a representative model. For later convenience, the values of several important quantities are summarized in Table II. The time evolution of the amplitude of gravitational wave and the central density near core bounce are shown in Figure 1. As the inner core shrinks, the central density increases and a core bounce occurs when the

central density reaches its peak at $t_b \cong 243$ msec with $2.65 \cdot 10^{14}$ g cm⁻³. At this time, the absolute value of the amplitude becomes maximum. After the core bounce, the core slightly re-expands and oscillates around its equilibrium. As a result, the gravitational wave shows several small bursts and begins to decay. These gross properties are common to all other models. However, there exist some important differences when we compare them in more detail. We will discuss the differences in the following.

In Figure 2, the time evolution of the amplitude of gravitational wave and the central density near core bounce for model MCS are given. For the model, it is noted that the initial rotation law is cylindrical with strong differential rotation. By comparing the left panel of Figure 1 to 2, the oscillation period of the inner core for model MCS is clearly longer than for model MSL. In other words, the pronounced peaks can be seen distinctively in this case. This is because the central density becomes more smaller after the distinct bursts (compare the right panels of Figure 1 to 2). This effect increases with the initial angular momentum (compare the left panel of Figure 2 to 3). It is also found that the signs of the values of the second peaks are negative for model MCS, on the other hand, positive for model MSL (compare the left panels of Figure 2 to 1). Note that we will speak of the second peak where the absolute amplitude is second largest. The above characteristics are common to the models for strongly differential rotation with cylindrical rotation law (see Table III). A specific feature in the waveform is found for models RSL and RSS in which there exist the small peak or shoulder before the peak burst (see the right panel of Figure 3).

Next we will compare our results of the waveforms with those by Zwerger et al. [12] who categorized the shapes of waveforms into three distinct classes. They used a polytropic EOS to express the pressure from the degenerate leptons as $P \propto \rho^\gamma$. They reduced the adiabatic index, γ , from 1.325 to 1.28 below the nuclear density regime in order to approximate the related microphysics and neutrino transport. They assumed the cylindrical rotation law for all the models and varied both the degree of differential rotation and the initial angular momentum. Our models except for the strongly differential rotation with cylindrical rotation law correspond to so-called the type I in their nomenclature. On the other hand, our models for strongly differential rotation with cylindrical (not shellular) rotation law correspond to type II. It should be noted that type II signals were limited to occur only for rapid, strongly differential rotation with cylindrical rotation law in their models. Furthermore in this study, we find that type II does not occur for models with shellular rotation law regardless of the

TABLE III: Some characteristic quantities for the waveform analysis. The names of the models whose initial rotation law is cylindrical with strong differential rotation are written in bold letters. T_{osc}^I and T_{osc}^{II} the first and second oscillation period of the inner core, respectively. h_{second}^{TT} is the amplitude of gravitational wave at the second peak.

Model	T_{osc}^I	T_{osc}^{II}	h_{second}^{TT}
	[ms]	[ms]	[10^{-20}]
SSL	1.6	2.4	0.82
SSS	1.5	2.2	0.94
SCL	1.6	2.3	0.75
SCS	1.8	2.6	-0.57
MSL	1.8	1.2	1.23
MSS	2.2	2.4	0.98
MCL	1.7	1.1	1.20
MCS	3.1	2.6	-0.79
RSL	1.0	3.1	0.32
RSS	1.0	7.8	0.20
RCL	9.0	2.9	0.25
RCS	10.7	8.6	-0.49

degree of differential rotation and the initial rotation rate, on the other hand, does occur regardless of the initial rotation rate in case of strong differential rotation with cylindrical rotation law. Finally type III occurred only when the core collapses very rapidly ($\gamma = 1.28$) in their calculations. There are no models which correspond to the type in our calculations. This is because our realistic EOS is not so soft in the corresponding density regime.

2. Maximum Amplitude and Second Peak

We will first discuss the relation between the maximum amplitudes of gravitational wave and the initial $T/|W|$. The maximum values and the related quantities are given in Table I and II. From Figure 4, it is found that the amplitude is largest for moderate initial

rotation rate (i.e., $T/|W|_{\text{init}} = 0.5\%$) when one fixes an initial rotation law and a degree of differential rotation. This is understood as follows. The amplitude of gravitational wave is roughly proportional to the inverse square of the typical dynamical scale, t_{dyn} (e.g., Eq. (3)). Since t_{dyn} is proportional to the inverse root of the central density ρ , the amplitude is proportional to the density. As a result, the amplitude becomes smaller as the initial rotation rates become larger because the density decreases for large initial rotation rate (see Table II and Figure 5). On the other hand, the amplitude is proportional to the value of the quadrupole moment, which becomes large in turn as the total angular momentum increases. This is because the stronger centrifugal forces make not only the mass of the inner core larger (see Table II), but also deforms the inner core. The amplitude is determined by the competition of these factors. As a result, the amplitude becomes extrema for moderate initial rotation rates in our calculation.

Next we will discuss the values of maximum amplitude between our results and those by other groups. The values of maximum amplitude for all our models range from $5 \times 10^{-21} \leq h^{\text{TT}} \leq 3 \times 10^{-20}$, which is almost the same as the results by Zwerger et al. [12] and Mönchmeyer et al. [10]. On the other hand, the values of the standard models by Yamada et al. [11] are about an order of magnitude lower. This is understood as follows. Yamada et al. [11] employed a parametric EOS by which the effects of microphysical and transport processes were assumed to be expressed. Since they found that the maximum amplitude is most sensitive to the adiabatic index at the subnuclear density by their parametric surveys, we pay attention to this. The comparison of the effective adiabatic index between our EOS and their EOS is shown in Figure 6. Compared to their EOS, our realistic EOS is rather soft for the subnuclear density regime. At the regime, our realistic EOS can express the softening of EOS by the effect that the nuclear interactions become attractive. Due to this effect, the inner core can shrink more compact at core bounce, which results in the larger maximum amplitude. It is naturally suggested that we may get the information about the subnuclear matter if we can detect the gravitational wave from the rotationally collapsing cores. We hope it can be realized in the near future since the maximum amplitudes for our models are mostly within the detection limit for TAMA and first LIGO which are now in operation if a source is located at a distance of 10 kpc (see Figure 7).

As pointed earlier, we find that the signs of the values of the second peaks are negative for the models for strongly differential rotation with cylindrical rotation law and positive for

the others (see Table III). The absolute amplitudes of the second peak are also presented in Figure 7. As shown, they are within the detection limit of first LIGO for a source at a distance of 10 kpc. In addition, it seems quite possible for the detectors in the next generation such as advanced LIGO and LCGT to detect the difference. Therefore if we can find the difference of the signs of the second peaks by observations of gravitational wave, we will obtain the information about the angular momentum distribution of evolved massive stars. Since there is no way except for the detection of the gravitational wave to obtain the information, it is of great importance to detect the second peaks in the future.

3. *Secular instability*

In some models (Models RSL and RCS) with large initial rotation rate, the final rotation rate exceeded the critical value (see Table II), where MacLaurin spheroids become secularly unstable against tri-axial perturbations ($T/|W| > T/|W|_{\text{seq}} = 13.75\%$). Rampp et al. [13] reported that no considerable enhancement of gravitational radiation due to the growth of secular instabilities was found within a time scale of several 10 ms after core bounce. Since our calculations are within the time scale, the axial symmetry assumed in this work may be justified.

IV. CONCLUSION

We have done a series of two-dimensional hydrodynamic simulations of the rotational collapse of a supernova core and calculated gravitational waveforms using the quadrupole formula. We have employed a realistic EOS and taken into account electron captures and neutrino transport in an approximated method. We have found the following:

1. The peak amplitudes of gravitational wave obtained in this study are mostly within the detection limits of the detectors of TAMA and first LIGO which are now in operation if a source is located at a distance of 10 kpc. In addition, the peak amplitude becomes extrema for the models whose initial rotation rate is moderate.
2. The waveforms are categorized into the criteria by Zwerger et al. [12]. In addition, we further find that type II does not occur for models with shellular rotation law, on the other hand, does occur regardless of the initial rotation rate in case of strong differential

rotation with cylindrical rotation law, and that the type III does not occur if a realistic EOS is employed.

3. At the subnuclear density regime, our realistic EOS can express the softening of EOS by the effect that the nuclear interactions become attractive. Therefore the inner core can shrink more compact at core bounce than the other work [11] in which EOS is expressed in a parametric manner. Subsequently, this results in the larger maximum amplitude. It follows that we may get the information about the subnuclear matter if we can detect the gravitational wave from the rotationally collapsing cores.

4. The signs of the values of the second peaks are negative for the models with strong differential rotation with the cylindrical rotation law, on the contrary, positive for the other models. The absolute amplitudes of the second peaks are within the detection limit of first LIGO. Therefore if we can detect the signs of the second peaks, it will give us the information as to the angular momentum distribution of massive evolved stars when a supernova occurs at our galactic center.

As stated earlier, the detection of gravitational wave is likely for the models whose initial rotation rate is moderate. According to the study of rotational core collapse by Kotake et al. [8], the anisotropic neutrino radiation is well induced by such a rotation rate. Noting that the anisotropic neutrino radiation can induce the globally asymmetric explosion [9], the detection of gravitational wave will be a good tool to help understand the explosion mechanism itself.

Acknowledgments

We are grateful to K. Numata and M. Ando for helpful discussions. K.K would like to be thankful to M. Oguri and M. Shimizu for supporting computer environments. The numerical calculations were partially done on the supercomputers in RIKEN and KEK (KEK supercomputer Projects No.02-87 and No.03-92). This work was partially supported by Grants-in-Aid for the Scientific Research from the Ministry of Education, Science and Culture of Japan through No.S 14102004, No. 14079202, and No. 14740166.

[1] C. Cutler and K. S. Thorne, to appear in Proceedings of GR16 (Durban, South Africa, 2001).

- [2] M. Cropper et al, Mon. Not. R. Astron. Soc. **231**, 695, (1988).
- [3] C. Papaliolis et al, Nature **338**, 13, (1989).
- [4] L. Wang et al, Astrophys. J. **579**, 671 (2002)
- [5] A. Lyne and D.R. Lorimer, Nature **369** (1994), 127.
- [6] J. L. Tassoul, 1978, *Theory of Rotating Stars* (Princeton: Princeton Univ. Press).
- [7] A. Heger, N. Langer and S. E. Woosley, Astrophys. J. **528**, 368, (2000).
- [8] K. Kotake, S. Yamada, and K. Sato, submitted to Astrophys. J.
- [9] T. M. Shimizu, T. Ebisuzaki, K. Sato, and S. Yamada, Astrophys. J. **552**, 756, (2001).
- [10] R. Mönchmeyer, G. Schäfer, E. Müller, and R. E. Kates, Astron. Astrophys. **246**, 417, (1991).
- [11] S. Yamada and K. Sato, Astrophys. J. **450**, 245, (1995).
- [12] T. Zweiger and E. Müller, Astron. Astrophys. **320**, 209, (1997).
- [13] M. Rampp, E. Müller, and M. Ruffert, Astron. Astrophys. **332**, 969R, (1998).
- [14] H. Dimmelman, J. A. Font, and E. Müller, Astron. Astrophys. **393**, 523D, (2002).
- [15] C. L. Fryer, D. E. Holz, and S. A. Hughes, Astrophys. J. **565**, 430, (2002)
- [16] M. Shibata, Phys. Rev. D. **67**, 024033 (2003).
- [17] K. S. New, accepted for publication in Living Reviews in Relativity, gr-qc/0206041.
- [18] C. L. Fryer and A. Heger, Astrophys. J. **541**, 1033, (2000).
- [19] J. M. Stone and M. L. Norman, Astrophys. J. Supl. **80**, 753, (1992).
- [20] R. I. Epstein, and C. J. Pethick, Astrophys. J. **243**, 1003, (1981).
- [21] S. A. Bludman, I. Lichtenstadt, and G. Hayden, Astrophys. J. **261**, 661, (1982).
- [22] K. A. van Riper, and J. M. Lattimer, Astrophys. J. **249**, 270, (1981).
- [23] K. A. van Riper, Astrophys. J. **257**, 793, (1982).
- [24] H. Shen, H. Toki, K. Oyamatsu, and K. Sumiyoshi, Nucl. Phys. **A637**, 43, (1998).
- [25] M. Ando and TAMA collaboration, Class. Quantum Grav. **19**, 1409, (2002).
- [26] K. S. Thorne, Gravitational Waves. In *Proceedings of the Snowmass 95 Summer Study on Particle and Nuclear Astrophysics and Cosmology*, World Scientific, pp. 398-425, (1995).
- [27] A. Weinstein, Class. Quantum Grav. **19**, 1575, (2002).
- [28] LCGT Collaboration, Int. J. Mod. Phys. D, **5**, 557, (1999).

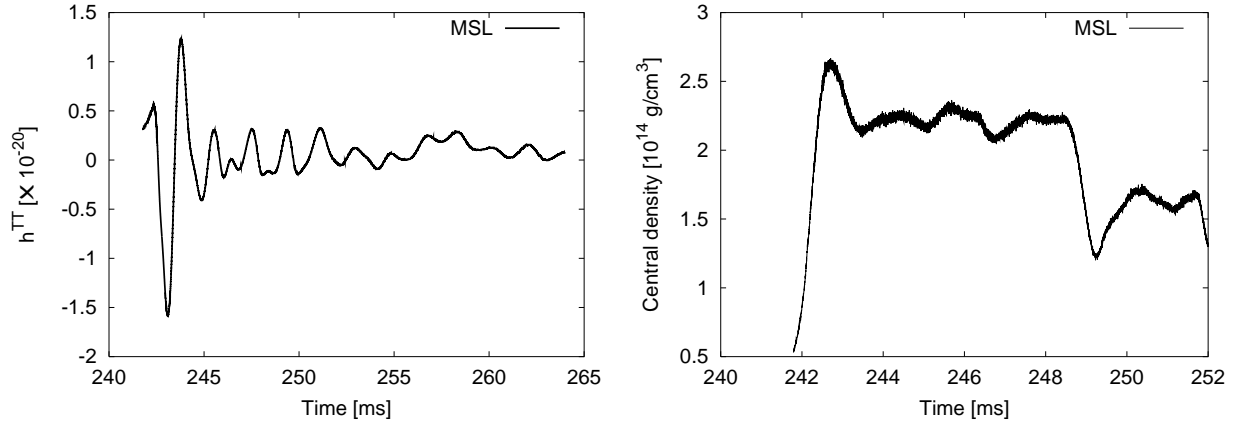


FIG. 1: Time evolution of the amplitude of gravitational wave (left panel) and central density near core bounce (right panel) for model MSL.

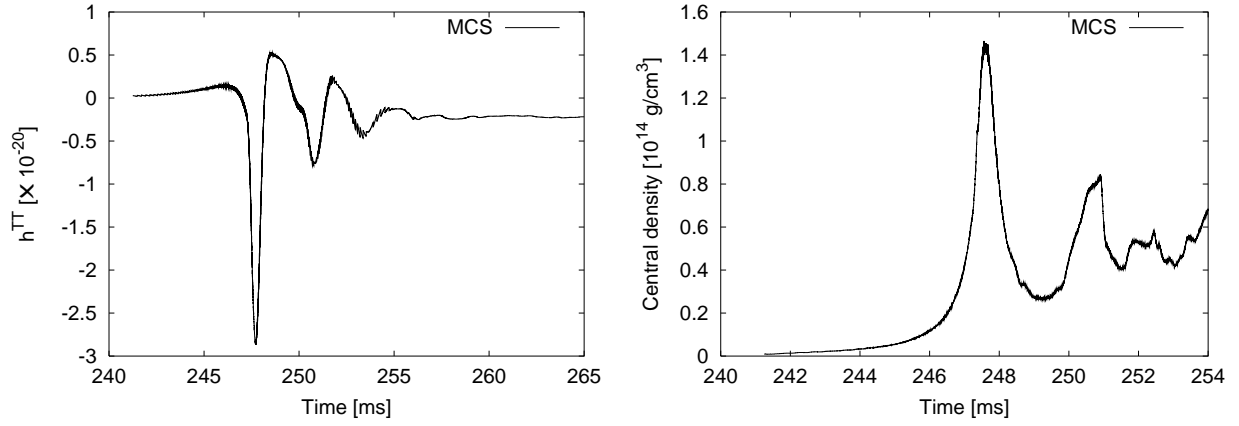


FIG. 2: Same as Figure 1 but for model MCS.

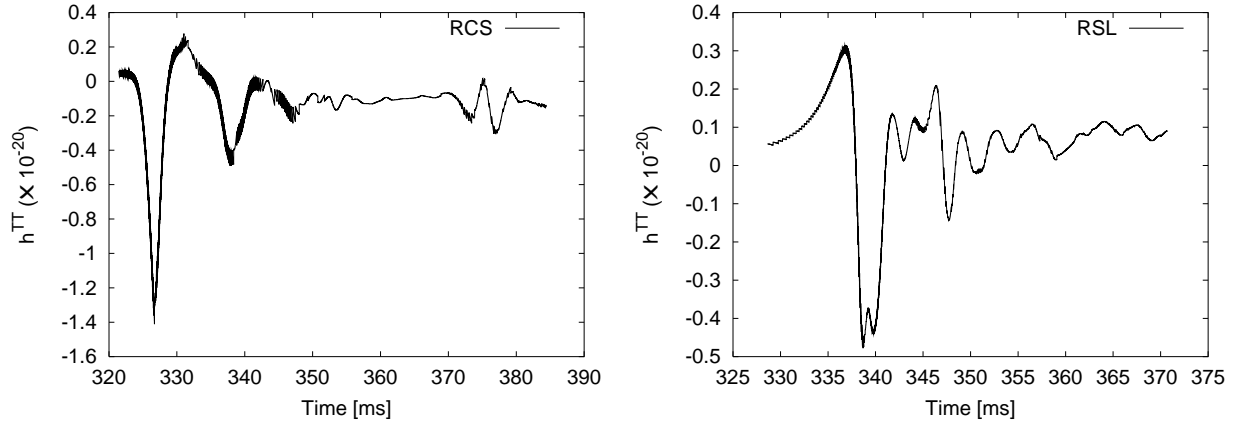


FIG. 3: Waveforms for models RCS (left panel) and RSL (right panel). For the left panel, very distinct peaks are shown. For the right panel, a small peak and shoulder after the first burst can be seen.

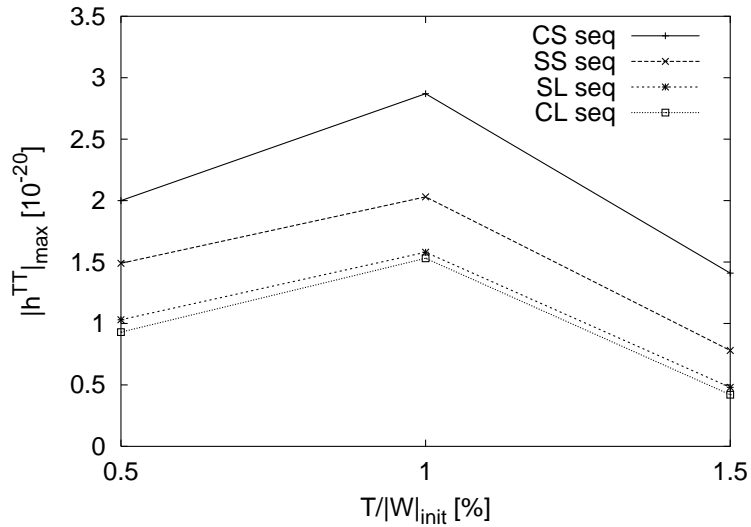


FIG. 4: Relation between $T/|W|_{\text{init}}$ and the peak amplitude $|h^{TT}|_{\text{max}}$ for all the models. “CS, SS, SL, CL seq” in the figure represent the model sequences whose names are taken from the second and third letters in Table I, respectively. Note that the second and third letters mean the rotation law and the degree of differential rotation, respectively.

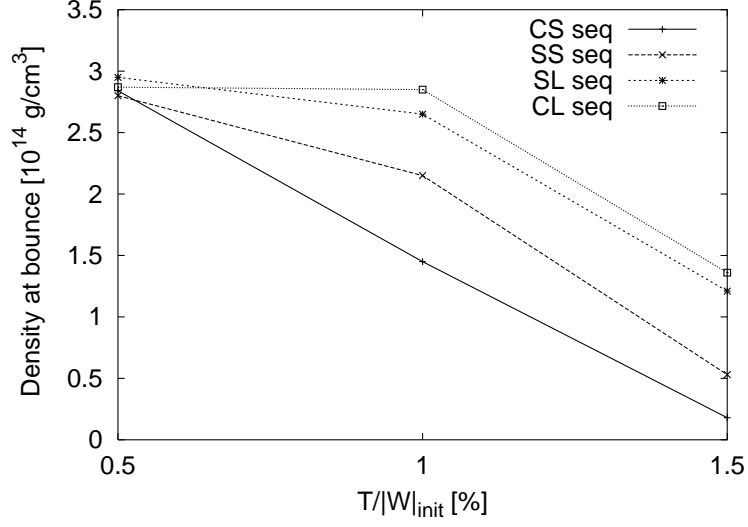


FIG. 5: Relation between $T/|W|_{\text{init}}$ and the central density at core bounce ($10^{14} \text{ g cm}^{-3}$) for all the models. The meaning of the label of lines is the same as Figure 4. It is found that the central density at the core bounce becomes smaller as the initial angular momentum becomes large.

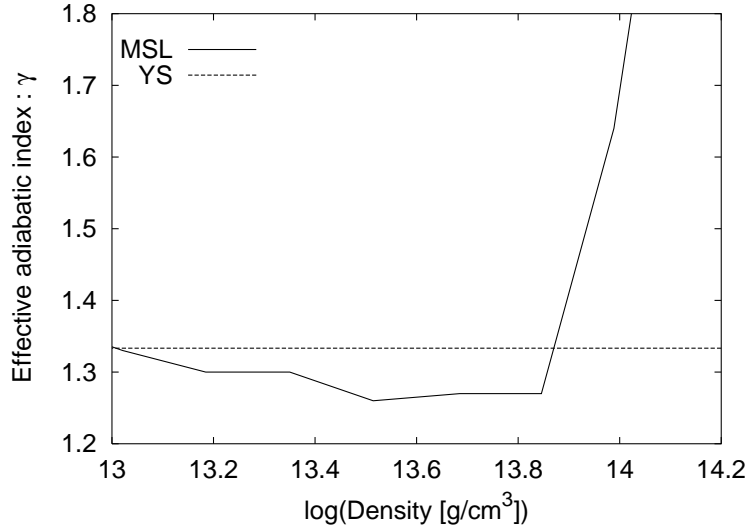


FIG. 6: Relation between the density and the effective adiabatic index γ at the subnuclear density. MSL represents the relation for our standard model. On the other hand, the index employed in the study of Yamada et al. [11] is represented as YS.

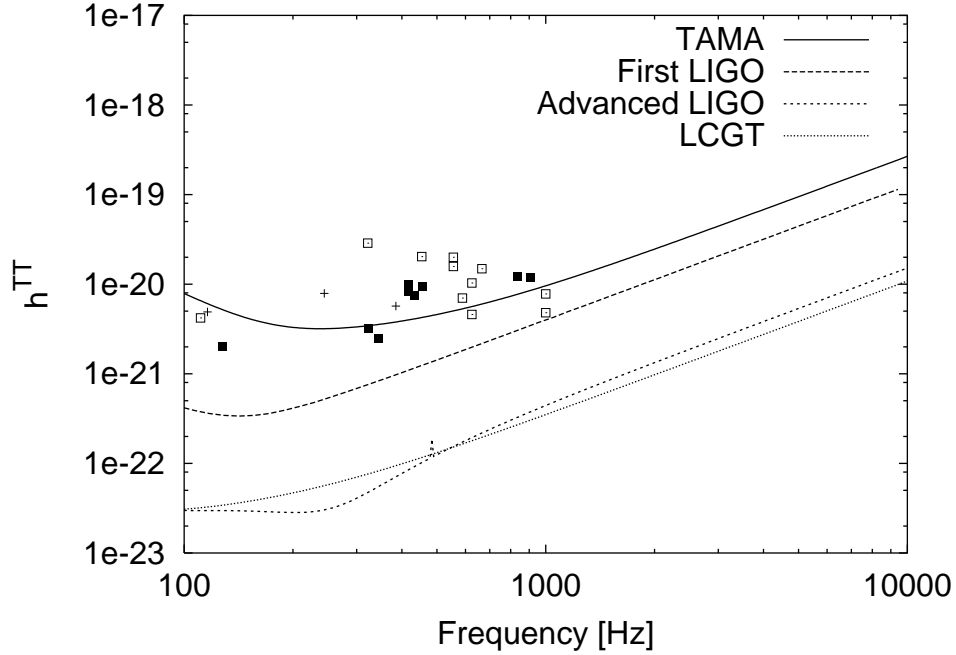


FIG. 7: Detection limits of TAMA [25], first LIGO [26], advanced LIGO [27], and LCGT [28] with the expected amplitudes from numerical simulations. The open squares represent the maximum amplitudes for all the models. On the other hand, the pluses and the closed squares represent the amplitudes of second peaks for models with strong differential rotation with cylindrical rotation law and for the other models, respectively. We estimate the characteristic frequencies by the inverse of duration periods of the corresponding peaks. Note that the source is assumed to be located at the distance of 10 kpc.